# Eruption-fed particle plumes and volcaniclastic deposits at a submarine volcano: NW Rota-1, Mariana Arc

Sharon L. Walker,[1] Edward T. Baker,[1] Joseph A. Resing,[2] William W. Chadwick Jr.,[3] Geoffrey T. Lebon,[2] John E. Lupton,[4] and Susan G. Merle[3]

[1] NW Rota-1 is an active submarine volcano in the Mariana Arc with a summit depth of 517 m and an explosively erupting volcanic vent southwest of the summit at a depth of 530–560 m. During a period of ongoing explosive eruptions, particle plumes surrounded the volcano and at least $3.3 \times 10^7$ m$^3$ of volcaniclastic material was deposited on the southern flank. Particle plumes over the summit were magmatic-hydrothermal in origin characterized by $^3$He enrichment, hydrothermal precipitates, and low pH values. Plumes at multiple depths below the summit surrounded the volcano and were composed overwhelmingly of fresh, glassy shards of basalt. Rare anhydrite particles were present, but there was a complete absence of other hydrothermal components in the deep plume samples. These short-lived anhydrite particles indicate the source of the deep plumes is from within or very near the eruptive vent, and the mechanism for transport down the flanks of the volcano must be far faster than settling of individual particles. The deep plumes most likely originated from sediment gravity flows generated by explosive eruptions or slope failure and landslides of unstable materials that had accumulated near the eruptive vent. Suspended sediments detach from the volcano slopes at multiple depths and are transported laterally up to tens of kilometers where they contribute to fall-out deposits in distal sediments. These observations link mechanisms for the transport of volcanic ash in the submarine environment to the types of deposits common in volcaniclastic aprons and fine ash layers in distal sediments.

## 1. Introduction

[2] Opportunities to directly observe explosive submarine volcanism and the syneruptive transport and deposition of its products are rare, so models of eruption dynamics are typically based on studies of volcaniclastic deposits. The characteristics of stratification, bed grading, clast morphology and boundaries between layers are used to infer eruptive styles, transport mechanisms and depositional environments [*White*, 2000; *Head and Wilson*, 2003; *White et al.*, 2003, and references therein]. Volcaniclastic deposits are common on the flanks of island and intraoceanic arc volcanoes and within sediments surrounding convergent plate margins [e.g., *Draut and Clift*, 2006; *Clift and Lee*, 1998; *Lee et al.*, 1995]. Some are fall-out deposits while others provide evidence for dispersal and deposition of eruptive products by sediment gravity flows. Turbidites result from gravity flows of fine sediments. Other sequences indicate sediment gravity flows cover a wide range of flow types and are important for building the volcaniclastic aprons surrounding many submarine volcanic edifices. Examples include volcaniclastic debris flows initiated by large-scale eruption-fed or mass wasting events [*Chadwick et al.*, 2005; *Wright*, 1996; *White*, 2000], pyroclastic flows that enter the ocean during subaerial eruptions [*Mandeville et al.*, 1996; *Chadwick et al.*, 2005; *Sigurdsson et al.*, 2006], and vertical density currents that form when dense concentrations of airborne ash accumulate at the ocean surface [*Manville and Wilson*, 2004; *Carey*, 1997; *Fiske et al.*, 1998]. The terminology for gravity flows, also called density flows or currents, is neither well established nor consistently used in the geological literature (see Appendix A) [e.g., *Middleton and Hampton*, 1976; *Mulder and Alexander*, 2001]. In this paper, we use the term "sediment gravity flows," as it is the most general term that encompasses the broad range of mass transport events, including turbidity currents. We follow the criteria of *Cas and Wright* [1991] that the term pyroclastic flow should be reserved for describing hot, gas-supported flows.

[1]Pacific Marine Environmental Laboratory, NOAA, Seattle, Washington, USA.

[2]Joint Institute for the Study of the Atmosphere and Ocean, University of Washington, Seattle, Washington, USA.

[3]Cooperative Institute for Marine Resources Studies, Oregon State University, Newport, Oregon, USA.

[4]Pacific Marine Environmental Laboratory, NOAA, Newport, Oregon, USA.

[3] A variety of processes can initiate sediment gravity flows at submarine arc volcanoes: the collapse of eruption columns, explosive destruction of lava domes, destabilization and remobilization of eruption products that have accumulated on steep slopes, and slope failure due to eruption-related seismic activity resulting in slides, slumps and flows on the flanks of volcanoes [*Kokelaar and Busby*, 1992; *Fryer et al.*, 1997; *Head and Wilson*, 2003; *Wright et al.*, 2008]. Materials transported by sediment gravity flows during volcanic eruptions can originate as juvenile eruptive products, previously deposited clasts and hemipelagic sediments, or a combination of primary and reworked sources. Radial patterns, braided channels, hummocks, ripples and sediment waves seen in the acoustic imagery of volcaniclastic aprons surrounding active submarine volcanoes indicate that, at the largest scales, sediment gravity flows are significant transport mechanisms for volcaniclastic products and can deposit these materials distally to tens of kilometers around the edifices [*Chadwick et al.*, 2005; *Embley et al.*, 2006b; *Fiske et al.*, 1998; *Wright*, 1996; *Draut and Clift*, 2006].

[4] Until now, studies of active submarine explosive eruptions have been limited to shallow volcanoes where eruptions have breached the surface or have affected surface waters sufficiently (i.e., discolored water or floating pumice) to indicate activity [e.g., *Fiske et al.*, 1998; *Chiminée et al.*, 1991; *Baker et al.*, 2002]. Close observations of an exploding volcano are normally impossible due to safety concerns [*Fiske et al.*, 1998]. *Baker et al.* [2002] measured the distribution and sampled tephra in the water column surrounding actively erupting Kavachi volcano in the Solomon Islands in May 2000. They found layers of fine-grained particles extending to depths greater than 1200 m, at distances at least 5 km from the shallow (2–5 m) summit. These layers were predominantly composed of shattered, ~3 $\mu$m mean diameter, unvesiculated glass particles with limited evidence (in only 2 of 22 samples) of dissolved or precipitated hydrothermal species (e.g., Fe or Mn) or magmatic gasses (e.g., $^3$He or $CO_2$), a contrast to event plumes sampled after mid-ocean ridge eruptions [*Baker et al.*, 1989; *Butterfield et al.*, 1997; *Feely et al.*, 1999; *Resing et al.*, 1999] or the observations at Macdonald seamount, an actively erupting hot spot volcano [*Chiminée et al.*, 1991]. *Baker et al.* [2002] concluded that most of the hydrothermal fluids and magmatic volatiles discharged during the Kavachi eruption were released directly to the atmosphere. Particle layers shallower than 250 m appeared to be directly emplaced by summit explosions and related base surges with highly directional dispersal controlled by local currents. The layers deeper than 250 m were more widespread, with particle concentrations near the seafloor often greater than in the shallower plumes. It was suggested that these particle layers could be the result of resuspension of previously deposited pyroclasts off the flanks of the volcano due to seismic energy [*Baker et al.*, 2002; *Fiske et al.*, 1998].

[5] In this paper, we describe only the second investigation of the production and dispersal of volcaniclastic materials at an actively erupting submarine volcano. NW Rota-1, on the Mariana Arc, differs importantly from Kavachi in several ways. First, a summit depth of ~550 m insures that the erupting material and its dispersal are confined completely to the submarine environment. Second, the hydrostatic pressure at that water depth is sufficient to suppress the energy of the eruption and allow close and prolonged visual inspection of the vent. Third, multiple and extended visits to NW Rota-1 over a 4-year period allow unprecedented long-term measurements of the production and dispersal of volcanic ash in the deep marine environment due to a continuing eruption. In addition, an area of volcaniclastic deposition on the flanks of NW Rota-1 was identified by repeat bathymetric surveys in 2003 and 2006.

## 2. Geological Setting

[6] The Mariana Arc lies west of the convergent margin between the Pacific and Philippine Sea plates in the western Pacific [*Stern et al.*, 2003] (Figure 1). Of the 52 submarine volcanic centers along the arc, at least 20 are hydrothermally active [*Baker et al.*, 2008]. NW Rota-1 is located about 60 km northwest of the island of Rota, Commonwealth of the Northern Mariana Islands. Hydrothermal activity on NW Rota-1 was discovered during the first NOAA Mariana Submarine Ring of Fire expedition in 2003 [*Embley et al.*, 2004]. Dives during subsequent expeditions with remotely operated vehicles (ROV; ROPOS in March/April 2004, Hyper-Dolfin in October 2005, and Jason II in April/May 2006) have provided an unprecedented opportunity for direct observations of explosive eruptive activity at a volcanic vent near the summit of the volcano [*Chadwick et al.*, 2008; *Embley et al.*, 2006a; *Deardorff et al.*, 2006].

[7] The volcanic edifice is steep-sided (with slope angles of 31° to water depths >1000 m), conical, basaltic to basaltic-andesite with a summit depth of 517 m (ROV depth sensor), and a basal diameter of about 16 km at 2700 m [*Embley et al.*, 2006a; *Chadwick et al.*, 2008]. Unstable deposits of volcaniclastic debris, sand, and talus cover the upper flanks of the volcano where evidence of large-scale mass wasting on the steep slopes is common.

[8] Brimstone Pit is the name of an active volcanic vent located approximately 45 m SW of the summit at a water depth of 530–560 m [*Embley et al.*, 2006a; *Chadwick et al.*, 2008]. Extensive ROV observations indicate that Brimstone Pit is the only source of high-temperature, particle-rich discharge on the summit, though smaller, diffuse, lower-temperature vents were found along the summit ridge [*Embley et al.*, 2006a] (videos available online at http://www.oceanexplorer.noaa.gov/explorations/04fire). Only mobile fauna have been found thriving near the summit at NW Rota-1 [*Limén et al.*, 2006], evidence of a rapidly changing and unstable seafloor environment.

[9] Brimstone Pit is a dynamic site under constant change [*Chadwick et al.*, 2008], including the loss of a significant portion of the crater rim between the 2004 and 2006 observations. Accumulation and collapse of eruption products in the immediate vicinity of the vent and other areas near the summit were observed during ROV dives in 2006. Sand-sized material on the steep slopes was easily disturbed by ROV operations, causing small, localized grain flows.

[10] The eruptive activity at Brimstone Pit observed in 2004 was characterized by a highly variable, sometimes surging plume with droplets of molten sulfur and basaltic ash, lapilli, and occasional bombs (>15 cm) falling from the plume after being ejected from the pit [*Embley et al.*, 2006a]. In 2006, activity varied from quiet emission of gas bubbles, to large sulfur-rich clouds billowing from the eruptive pit, to
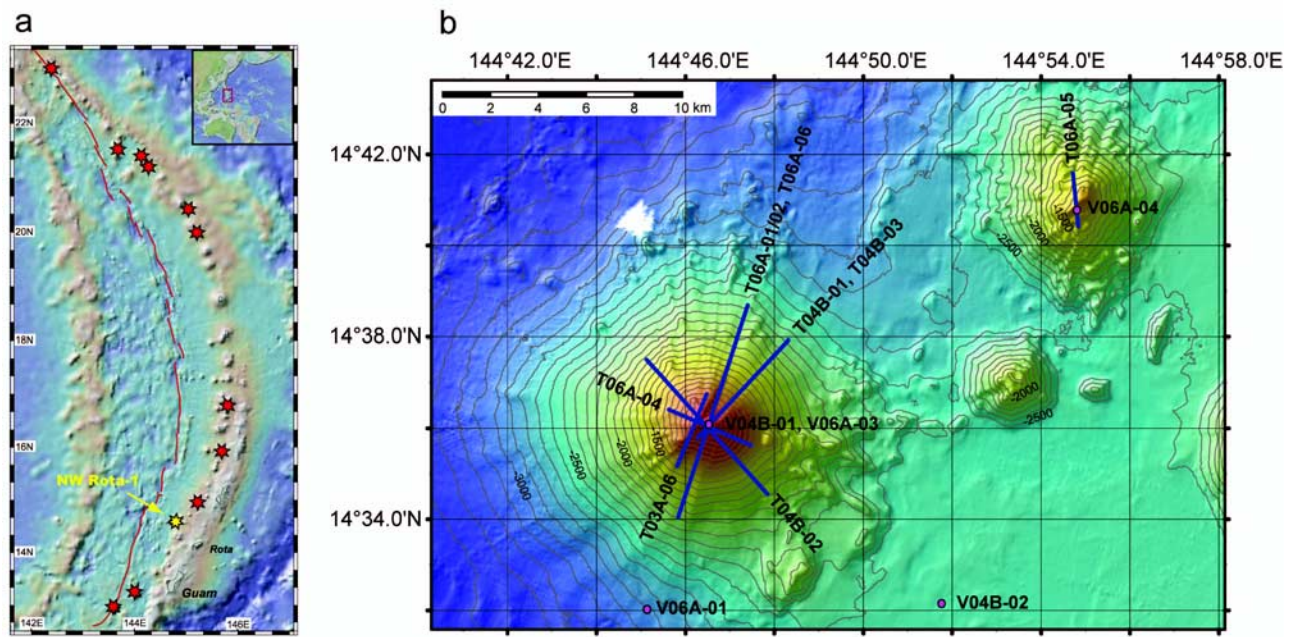
**Figure 1.** (a) Location and tectonic setting of NW Rota-1 (yellow star) and other hydrothermally active submarine volcanoes (red stars) along the Mariana volcanic arc. Red lines show location of back-arc spreading axis. (b) Track lines of CTDO tow-yos (lines) and vertical cast positions (circles) at NW Rota-1 in 2003 (CTD tow T03A-06), 2004 (CTD tows labeled "T04B-xx" and vertical casts labeled "V04B-xx," and 2006 (CTD tows labeled "T06A-xx" and vertical casts labeled "V06A-xx").

vigorous pulsating bursts of exploding gasses and red hot blocks of lava. Activity fluctuated between intense and quiescent phases on the scale of minutes to tens of minutes, and eruption rates were low ($1-100$ m$^3$ h$^{-1}$) [*Deardorff et al.*, 2006; *Chadwick et al.*, 2008]. The broader impacts of this eruptive activity were documented by repeated water column measurements and bathymetric (sonar) surveys around the volcano.

## 3. Methods

[11] Particle plumes in the water column around NW Rota-1 were mapped and sampled in 2003, 2004, and 2006 (Figure 1b) with conductivity-temperature-depth-optical (CTDO) vertical casts and "tow-yos" in accordance with the methods and equipment described by *Baker et al.* [1995]. Optical backscatter data are reported as $\Delta$NTU, dimensionless nephelometric turbidity units [*American Public Health Association*, 1985] above the regional background, which is correlated to suspended particulate mass concentration. The slope of the least squares regression between suspended particulate mass concentration and NTU is affected by mean particle size and composition and ranges from $\sim$0.11 L mg$^{-1}$ for aluminosilicates with a mean diameter of 29 $\mu$m to $\sim$2.5 L mg$^{-1}$ for hydrothermal iron oxyhydroxide precipitates, and greater for particle populations dominated by particulate sulfur [*Baker et al.*, 2001; *Feely et al.*, 1999]. Water samples for chemical analysis were collected with 19-L Niskin-type bottles while monitoring the real-time display of $\Delta$NTU. Samples were analyzed for helium isotopes ($^3$He and $^4$He [*Lupton and Craig*, 1975]), pH (a proxy for $CO_2$ and other acidic magmatic volatiles [*Resing et al.*, 1999]), particulate elemental composition

[*Feely et al.*, 1999], and the morphology of individual particles by scanning electron microscopy (SEM). Short-term temporal changes were observed by repeat tows separated by 3–6 days in 2004 and 2006.

[12] Depth differences at NW Rota-1 were determined by repeat multibeam sonar bathymetry surveys conducted in February 2003 and April 2006. The 2003 survey was collected with the 30 kHz EM300 system on the R/V *Thompson*, the 2006 survey with the 12 kHz Seabeam2000 system on the R/V *Melville*. Both surveys were navigated by DGPS and corrected for sound velocity calculated from concurrent CTD data. Quantitative comparison of the two surveys generally followed the method described by *Fox et al.* [1992] and *Wright et al.* [2008]. Each survey was gridded separately with a 30 m cell size and the grids subtracted to generate a raw difference grid. Raw difference grids contain false differences due to slope-dependent errors in position and depth and the lower quality of the Seabeam2000 data. To distinguish signal from noise, significant depth differences were determined as those above an empirical threshold after weighting raw differences as a function of slope.

## 4. Depth Changes Between 2003 and 2006

[13] Comparison of the two multibeam bathymetry surveys (Figure 2) from 2003 and 2006 shows significant depth differences up to 40 m located immediately downslope of the eruptive vent, Brimstone Pit. The raw difference grid is somewhat noisy (Figure 2c), but includes a swath of positive depth change on the south flank of the volcano and generally negative depth changes elsewhere. After applying the slope-dependent weighting factor and
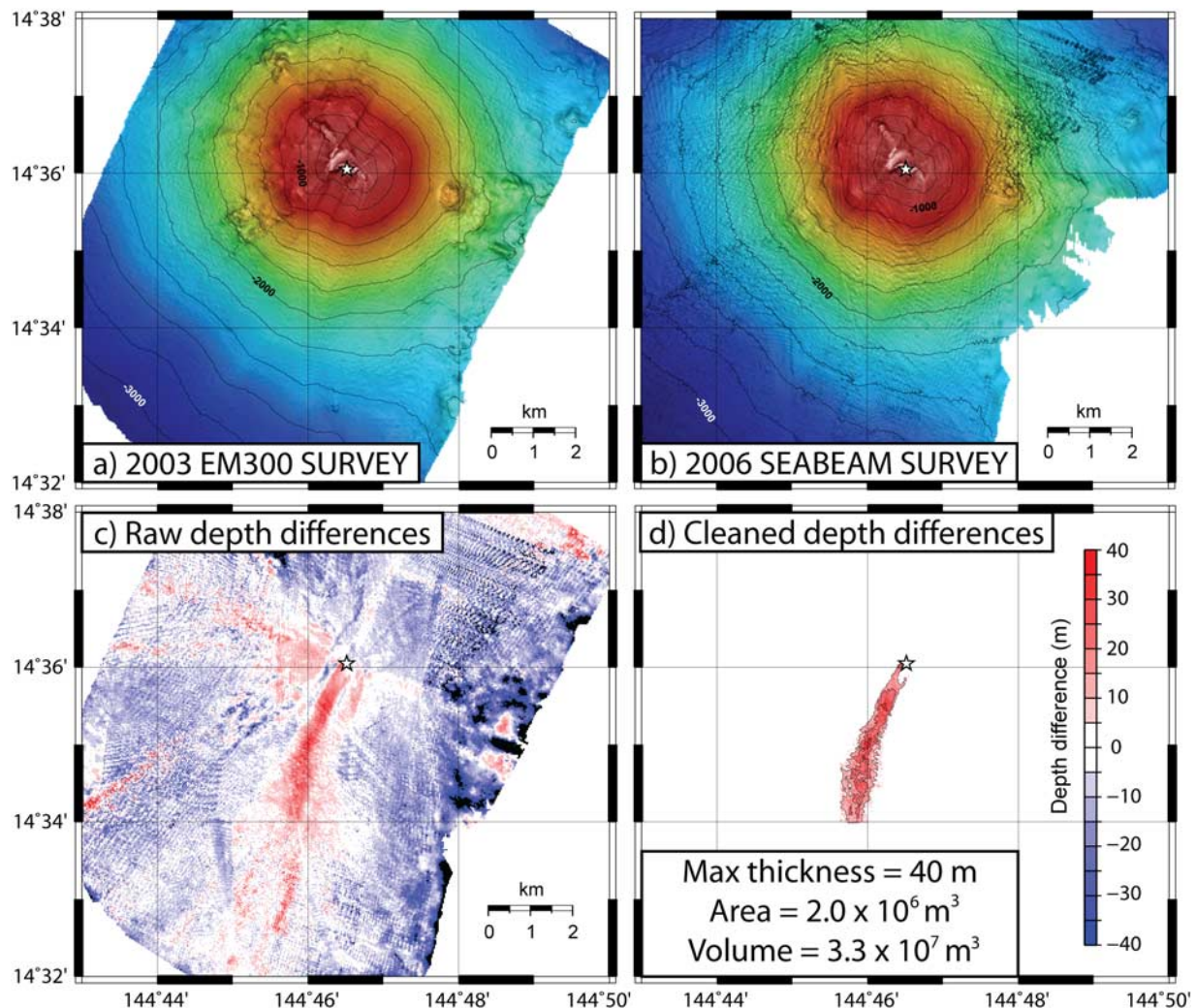
**Figure 2.** Depth changes between multibeam surveys at NW Rota-1. (a) EM300 survey from R/V *Thompson* in 2003. (b) Seabeam2000 survey from R/V *Melville* in 2006. (c) Raw depth differences between the two surveys. (d) Cleaned depth differences with 10-m contours. Star indicates location of Brimstone Pit eruptive vent. Positive depth differences reflect the accumulation of volcaniclastic materials.

empirical threshold, the positive swath was interpreted to be the only significant area of depth change, as shown in the final cleaned difference grid (Figure 2d). The positive swath extends to at least the 2000 m bathymetric contour (a horizontal distance of 4 km from the summit). Its lateral extent is constrained within a low-relief chute formed by two inward facing normal faults that are oriented NE-SW and cut across the summit of the volcano. The area and volume of depth change in the cleaned difference grid are $2.0 \times 10^6$ m$^2$ and $3.3 \times 10^7$ m$^3$, respectively.

[14] The area of positive depth change is interpreted to be volcaniclastic material deposited downslope from Brimstone Pit between 2003 and 2006 as the result of eruptive activity at the vent. The volume of the deposit is consistent with the volcano being more or less continuously active between 2003 and 2006 at about the same rate that was observed in 2006 ($1-100$ m$^3$ h$^{-1}$) [*Chadwick et al.*, 2008], however, the emplacement of volcaniclastic deposits below Brimstone Pit is probably episodic.

[15] The location of the deposit is consistent with emplacement by sediment gravity flows, most likely gen-erated by landsliding when the cone of accumulated ejecta surrounding the active vent becomes unstable and period-ically collapses [*Chadwick et al.*, 2008]. Recent ejecta (bombs, lapilli and ash) and distinct slide chutes were observed on the slope tens of meters below Brimstone Pit during dives with the ROV in 2006 [*Chadwick et al.*, 2008]. Additionally, a sediment gravity flow due to eruption column collapse was observed during ROV operations after a sudden explosion at the vent. The flow was a fast moving (0.3 m s$^{-1}$) cloud hugging the seafloor as it moved toward the ROV (Figure 3) [see also *Chadwick et al.* [2008, Movie 7].

## 5. Plume Distributions

[16] NW Rota-1 is unusual compared with other hydro-thermally active arc volcanoes because particle plumes occur here in two spatially and chemically distinct environ-ments. As at other hydrothermally active volcanoes, the summit discharge creates a plume layer with a rich chemical burden that rises buoyantly and spreads laterally within a narrow depth interval. In addition, deep-water particle
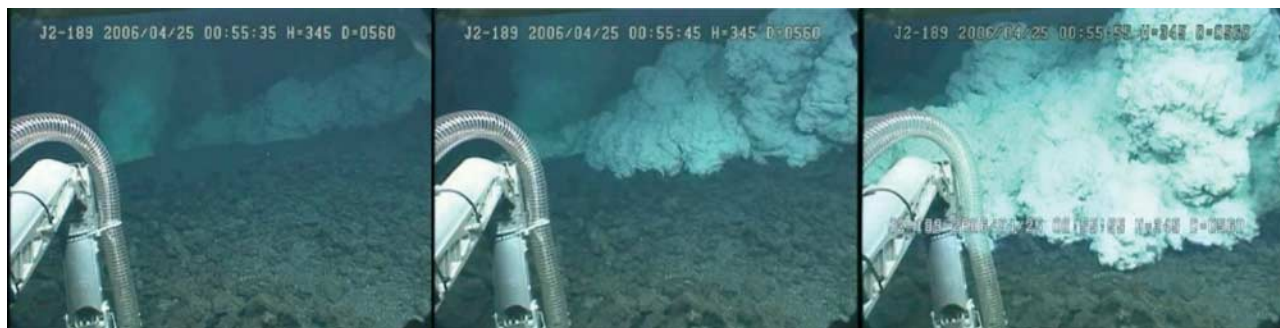
**Figure 3.** A fast moving plume during vigorous explosive eruptions at Brimstone Pit observed overflowing the rim and moving downslope as a sediment gravity flow (frames are from video at 10-s intervals) (video available at http://www.oceanexplorer.noaa.gov/explorations/06fire/logs/april25/media/nwrota_brimstone6.html or Movie 7 of *Chadwick et al.* [2008]).

layers were found at multiple depths below the summit and surrounding the flanks of this volcano to depths >2500 m in 2004 and 2006. These layers extend for several kilometers beyond the volcano and lack the chemical characteristics of hydrothermal plumes. Deep plumes are composed primarily of volcanic ash, suggesting they are emplaced by sediment gravity flows concurrent with the volcanic eruption, thereby transporting fine ash both downslope along the volcano flanks and supplying a source of ash to the water column where it is subject to transport via regional currents and deposition in distal fall-out deposits.

### 5.1. Buoyant Hydrothermal-Magmatic Plumes

[17] Particle plumes over the summit of NW Rota-1 were optically intense (maximum $\Delta NTU$ values near the upper limit of the optical sensor) within a limited depth range (20–30 m thick) centered at 460 m water depth in 2003, 485 m in 2004, and 505–530 m in 2006 (Figures 4, 5, and 6). The particles were composed predominantly of hydrothermal precipitates including iron oxyhydroxides, Al sulfates, and elemental sulfur [*Lebon et al.*, 2004; *Resing et al.*, 2007] (Figure 7). These plumes were also enriched in $^3$He and had anomalously low pH due to the addition of magmatic $CO_2$ and acid (Figure 7) [*Resing et al.*, 2007]. The presence of particulate natroalunite [*Lebon et al.*, 2004; *Resing et al.*, 2007], which forms in high-temperature acidic fluids, is additional evidence of strong magmatic contribution [*de Ronde et al.*, 2005] to this hydrothermal system.

[18] A lower Fe/Si ratio in 2004 compared to 2003 and 2006 (Figure 8) is due to a greater fraction of rock fragments and reprecipitated Si in this particle population [*Lebon et al.*, 2004]. Rock fragments were highly corroded and depleted in Na, Mg, K, and Ca, with some dissolution of Al, Si, and Fe leaving unusually high Ti/Si ratios [*Lebon et al.*, 2004]. The presence of these types of particles in 2004, but not 2003 nor 2006, along with a more extreme pH anomaly ($\sim$−1.5 pH units in 2004 compared to $\sim$−0.7 in 2003 and 2006), suggests 2004 might have been a period of increased magmatic gas influx, and perhaps marks the beginning of an explosive eruption phase that perturbed the hydrothermal system. Magma-derived acids accelerate the alteration of host rocks and the onset of explosive eruptive activity may have contributed to shattering the altered rock lining the hydrothermal pathways causing these particles to be ejected into the summit plume.

### 5.2. Deep-Water Ash Plumes

[19] Deep plumes were absent in 2003 when hydrothermal activity was first discovered on NW Rota-1 but were present in 2004 and 2006. A deep water column survey was not conducted in 2005 so the presence or extent of deep plumes at that time is unknown. The plumes in 2004 and 2006 consisted of extensive particle layers at multiple depths greater than at least 600 m in all directions around the flanks of the volcano and were detectable as far as 18 km from the summit (Figures 5 and 6). Particle concentrations were often most intense near the seafloor. Intermediate layers appeared to originate at the flanks, spreading laterally on isopycnal surfaces at several depths. Repeat tows along a SW-NE transect (Figures 5 and 6; 2004 tows T04B-01 and T04B-03; 2006 tows T06A-01/02 and T06A-06) showed significant decreases in particle concentrations and a deepening of the upper limits of the deep plumes on the scale of 3–6 days, implying rapid settling and/or advection of the suspended particulates in these layers, and episodic emplacement.
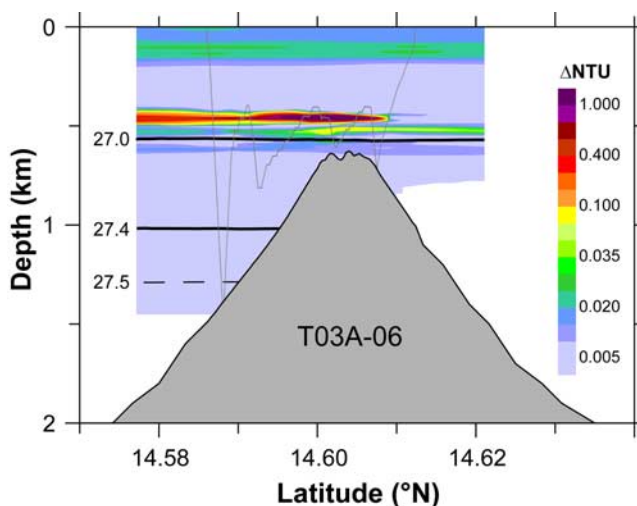


**Figure 4.** Particle plume distributions at NW Rota-1 in 2003. The saw-toothed tow path of the CTD during tow-yos is shown (light gray lines). Potential density contours are labeled solid and dashed black lines (contour intervals are variable).

[20] The deep plumes were composed overwhelmingly of fresh, shards of basalt glass, with occasional anhydrite crystals (Figures 8 and 9). Many of the individual glass particles examined were highly vesiculated or were bubble wall fragments (Figures 9a and 9b), indicating that lava-seawater interactions or rapid expansion and exsolution of magmatic gasses played a role in the fragmentation of these particles [Clague et al., 2000, 2003]. Hydrothermal indicators such as [3]He, Fe, and Mn oxyhydroxides and elemental sulfur were not present in deep plume samples (Figures 7 and 8) and rule out hydrothermal vents on the

flanks of the volcano as possible sources. Bulk chemistry and SEM photos reveal that the deep plume particle samples are remarkably similar from all depths, implying a common source and little sorting during transport.

## 6. Origin of the Deep Plumes

[21] More than 100 arc volcanoes have been surveyed for hydrothermal activity [e.g., de Ronde et al., 2003, 2007; Baker et al., 2008] and deep plumes have been observed only around two: Kavachi, in the Solomon arc [Baker et al., 2002], and NW Rota-1. These are also the only two known to be erupting while being surveyed. This shared characteristic implies that deep plumes are not simply the product of resuspension up and down the volcano flanks, but instead represent an ash transport mechanism initiated by the eruption process itself. In addition to the lack of hydrothermal particulates in the plumes, another clue provides evidence that this mechanism is not simply individual particles settling from the buoyant plume above the summit. At least two deep plume samples (as deep as 2065 m and as far as 4 km from the summit) contained individual anhydrite particles (Figure 9f). Anhydrite precipitates from seawater within a temperature range of $\sim150-300°C$ [Bowers et al., 1985; Kuhn et al., 2003] and dissolves rapidly in ambient seawater: a particle with a minimum linear dimension of $\sim50$ $\mu$m (as in Figure 9f) will completely dissolve in about 9 days in $2.0°C$ seawater (taking into account that in situ dissolution rates are about an order of magnitude slower than laboratory rates [Feely et al., 1987]). But all the anhydrite particles we sampled showed sharp edges, angular joints, and smooth surfaces, evidence that little dissolution had yet occurred.

[22] The only source for anhydrite at NW Rota-1 is precipitation in high-temperature hydrothermal fluids or as a result of lava-seawater interaction, both occurring only at the summit of the volcano. Anhydrite particles with an equivalent spherical diameter of 50 $\mu$m (as in Figure 9f) require approximately 10 days to settle from the depth of origin ($\sim550$ m) to the sample depth (2065 m) via Stokes settling alone (settling velocity calculated by Stokes Law is $V_s = (2/9)(a^2(\sigma - \rho)g/\eta)$, where $a$ is particle radius (m), $g$ is
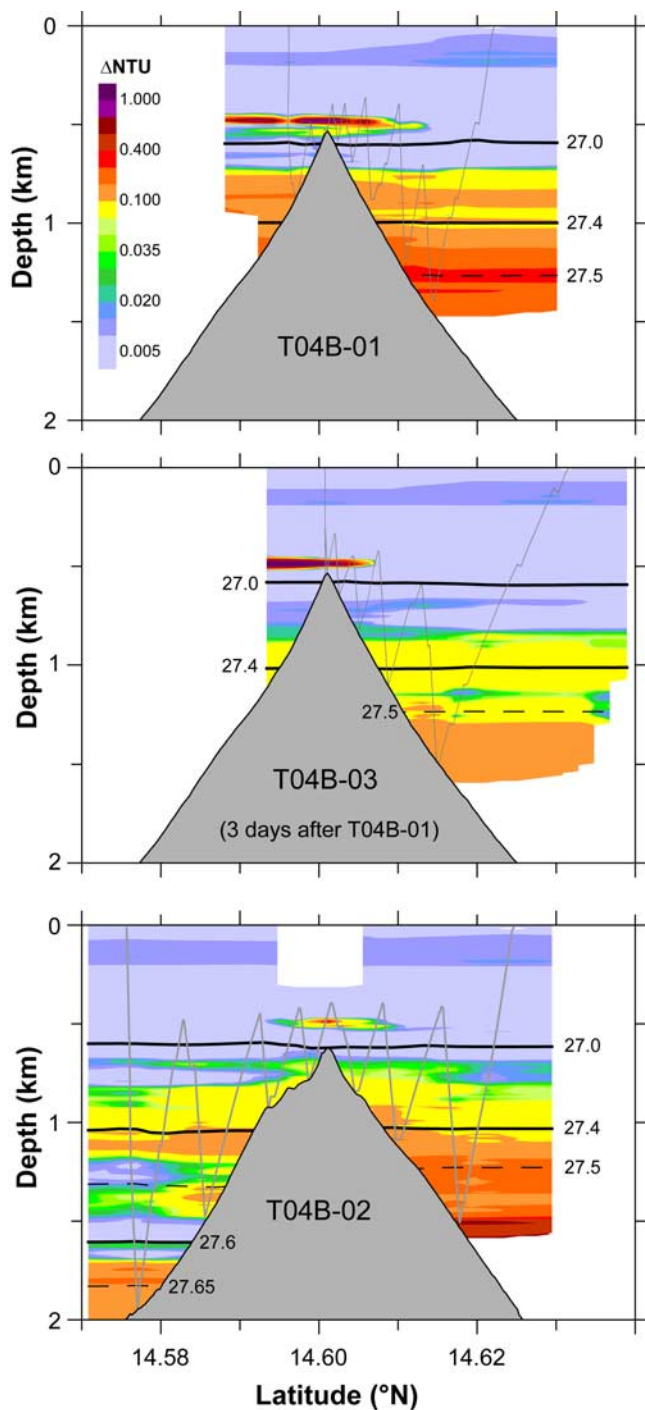


**Figure 5.** Particle plume distributions at NW Rota-1 in 2004. The saw-toothed tow path of the CTD during tow-yos is shown (light gray lines). Potential density contours are labeled solid and dashed black lines (contour intervals are variable). Tow T04B-03 repeated the path of and was conducted 3 days later than tow T04B-01. Tow T04B-02 is oriented orthogonal to the track lines of T04B-01 and T04B-03 (see Figure 1). The vertical distance spanned by the depth range of the particle plumes ($\sim400$ m to >2000 m water depth) resulted in wider horizontal spacing of up-down cycles along the flanks and closer spacing over the summit. Note that what appear to be particle-free regions at some depths below 1000 m are probably artifacts of the gridding and contouring parameters that were used for interpolation between data points. The most intense particle concentrations are usually nearest the seafloor, so particle clouds along the slope are probably more continuous than shown here.
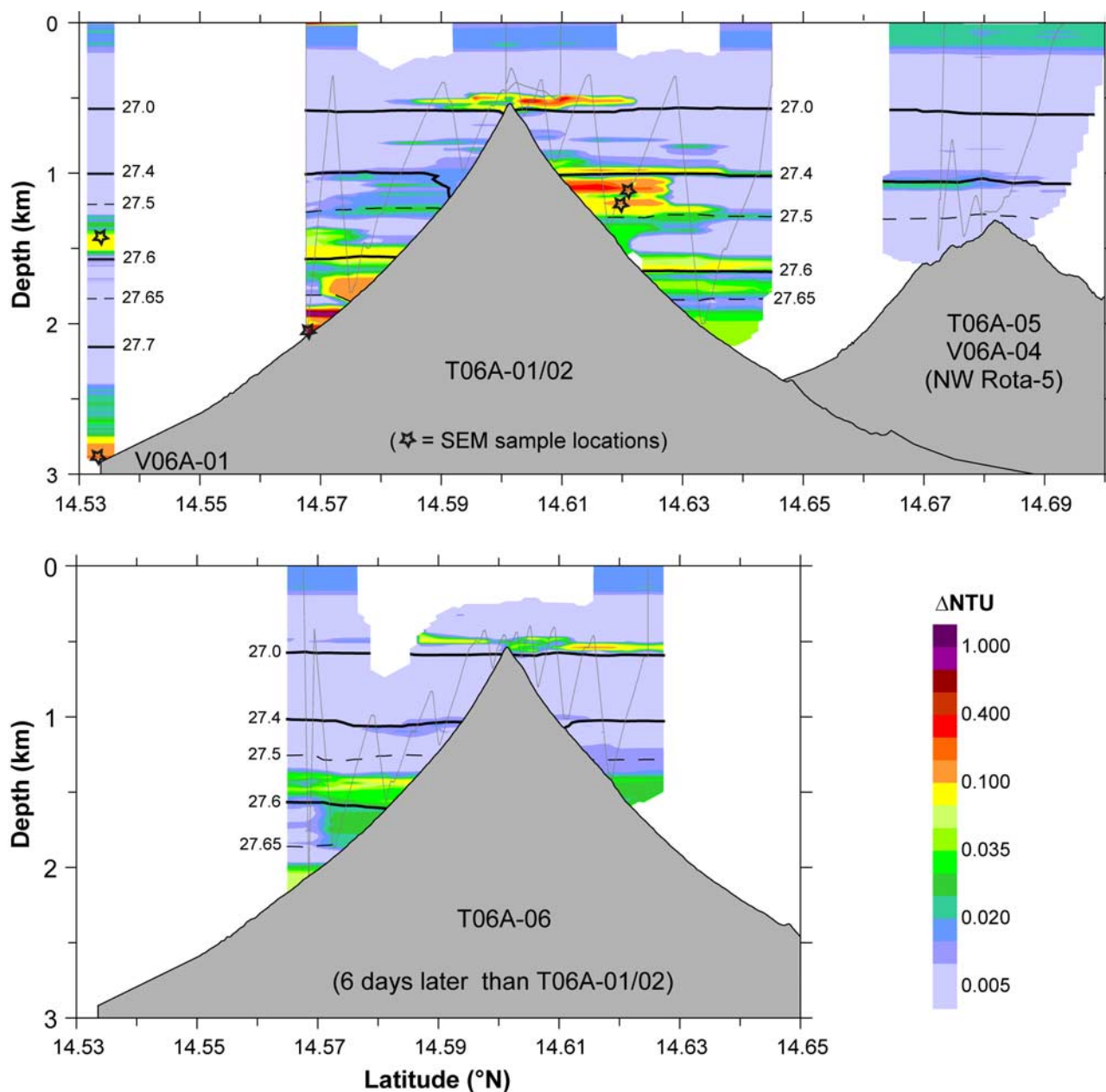
**Figure 6.** Particle plume distributions at NW Rota-1 in 2006. The saw-toothed tow path of the CTD during tow-yos is shown (light gray lines). Potential density contours are labeled solid and dashed black lines (contour intervals are variable). Stars locate the SEM samples shown in Figure 9. Tow T06A-06 repeated the path of and was conducted 6 days later than tow T06A-01/02. Some particle-free regions at depths below 1000 m are probably artifacts due to the wider horizontal spacing of up-down cycles along the flanks (as in Figure 5). The most intense particle concentrations are usually nearest the seafloor, so particle clouds along the slope are probably more continuous than shown here.

gravity (9.81 m s$^{-2}$); $\rho$ is fluid density; $\sigma$ is particle density (specific gravity of anhydrite is 2.97); and $\eta$ is dynamic viscosity (for seawater ~1.5 × 10$^{-3}$ N s m$^{-2}$ at 5°C)), an estimate that does not include the unknown period of time required for horizontal advection away from the volcano. The combined settling and advection time for anhydrite particles observed in these samples should have been sufficient for extensive, if not complete, dissolution. The observation of particles showing no signs of extensive dissolution demonstrates they were subject to a transport

mechanism far faster than simple advection and Stokes settling.

[23] Sediment gravity flow events initiated by the eruptions at Brimstone Pit are the best candidate for the required transport mechanism. Most of our water column observations are probably limited to the more diffuse, outer limits (in both space and time) of a sediment gravity flow, but at least three criteria suggest some of our observations may have been made shortly after the onset of such events: maximum particle concentrations mostly occurred near the
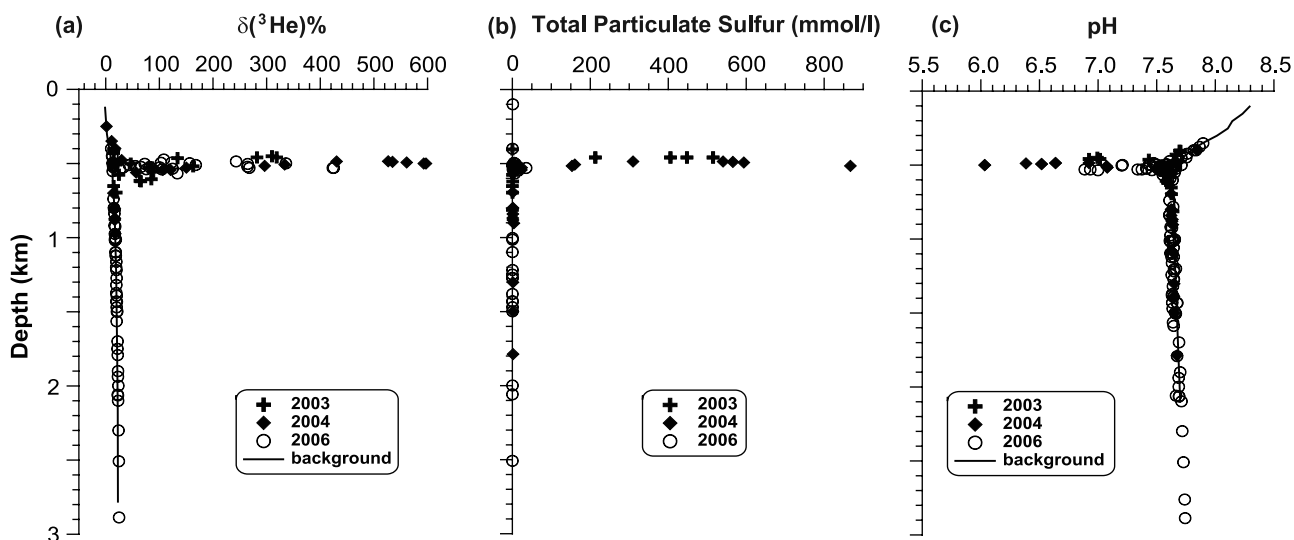
**Figure 7.** Profiles of (a) helium (as percent increase in the value for $^3$He/$^4$He above that in air; $\delta^3$(He)% = $100[(R/R_A) - 1]$, where $R$ is the $^3$He/$^4$He value of the sample and $R_A$ is the ratio in air), (b) total particulate sulfur, and (c) pH for all NW Rota-1 samples from 2003, 2004, and 2006. Background profiles (lines) for $\delta^3$(He)% and pH are from samples unaffected by particle plumes.

seafloor; anhydrite particles showing signs of only slight modification or dissolution were present in deep plume samples; and there was a decrease in near-bottom density for at least one tow-yo excursion, which could indicate shallower water being drawn downslope (Figure 10) by a sediment gravity flow.

[24] Gravitational collapse of eruption columns, failure of unstable deposits accumulating on the steep slopes near the vent, and explosive destruction of lava plugs and nearby deposits are possible mechanisms for initiating gravity flows during the eruptions at Brimstone Pit. The upper slopes of NW Rota-1 are quite steep (31° from the summit to about 1000 m) and eruptive products accumulating in the vicinity of Brimstone Pit have been observed to exceed the angle of repose [*Chadwick et al.*, 2008]. The finer fractions of these deposits are composed of volcaniclastic ash and sands with noticeable amounts of elemental sulfur spherules [*Chadwick et al.*, 2008]. Changes of the crater rim depth between 2004 and 2006 (with buildup of ∼20 m between 2004 and 2005, then loss of ∼30 m by the 2006 observations) demonstrate the dynamic accumulation and loss of these deposits. Landsliding of these deposits is another type of sediment gravity flow.

[25] Slope failures from deeper on the flanks of the volcano or generalized resuspension due to seismic energy are considered less likely sources because of the presence of short-lived anhydrite crystals in the deep plumes. These particles strongly suggest the source materials for these plumes must come from the summit at, or very near, Brimstone Pit where anhydrite can form and might persist for a short time. It is probably impossible to distinguish ash that enters a sediment gravity flow due to slope failure of near-vent material from ash particles entrained in the collapse of an eruption column or created by an intense explosion at the mouth of the vent.

[26] It is interesting to note the complete absence of elemental sulfur in deep plume samples despite its prominence in the buoyant, yellow-white plume rising from

Brimstone Pit, in the plumes over the summit, and in the fine materials deposited on the seafloor near the vent and elsewhere around the summit of NW Rota-1 [*Chadwick et al.*, 2008]. Elemental sulfur might be absent from the deep
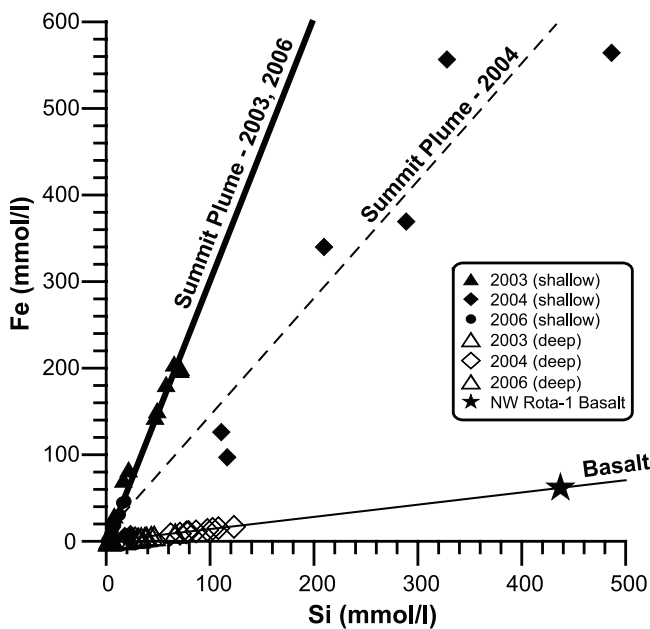


**Figure 8.** Fe/Si ratio of plume particles in the magmatic-hydrothermal plumes over the summit of NW Rota-1 (shallow samples) compared to those of deep plume samples in 2003, 2004, and 2006. The predominant form of iron in the summit plumes is as Fe oxyhydroxide, a hydrothermal precipitate. Silica is a relatively stable component of basalt rocks, so the average Fe/Si ratio of the bulk particulate samples is useful for characterizing plume particulates as predominantly hydrothermal or basaltic. The Fe/Si ratio of magmatic-hydrothermal plume particles in 2004 was anomalous due to a greater percentage of highly corroded rock particles in that population compared to 2003 or 2006.
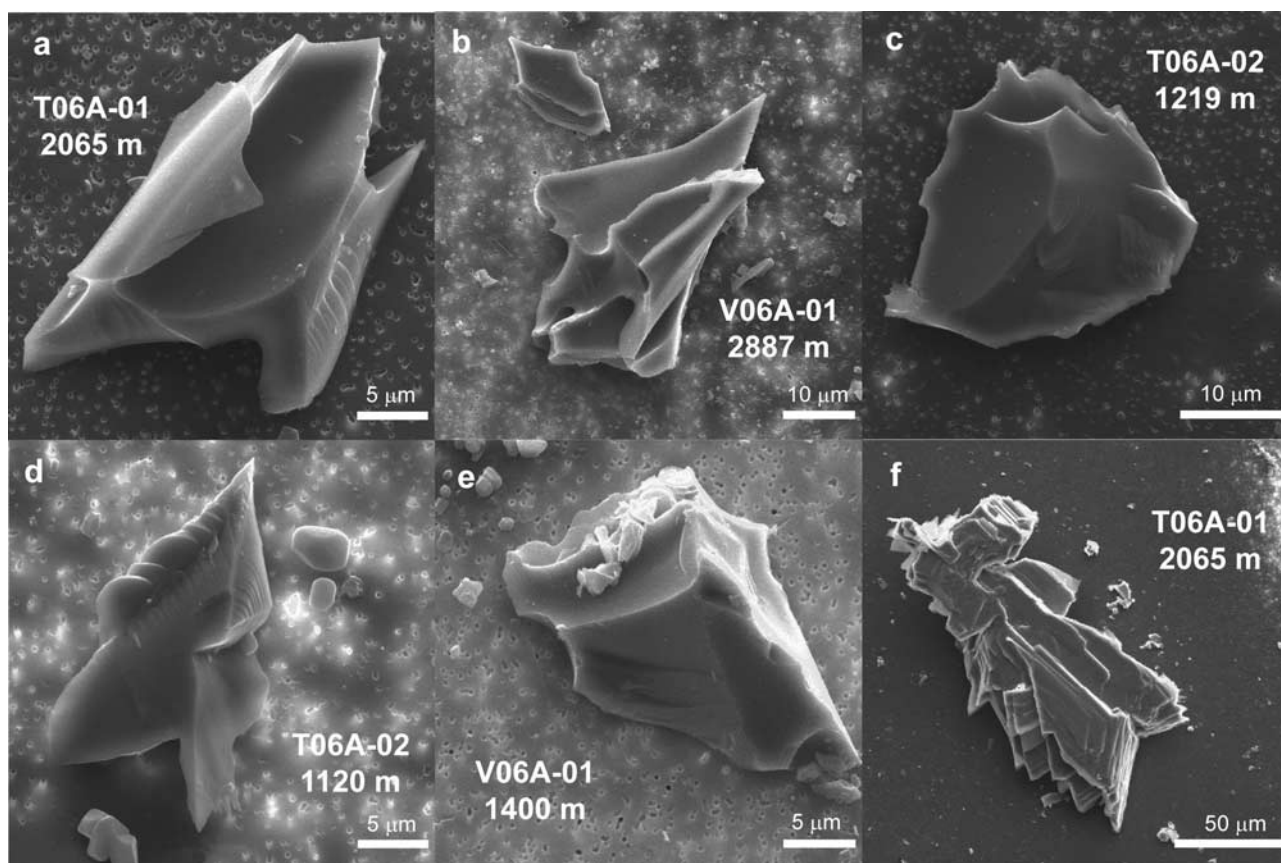
**Figure 9.** SEM micrographs of representative glassy basalt shards from deep plumes (sample locations indicated by stars in Figure 6). The particles consisted of (a and b) highly vesiculated particles, (c) bubble wall fragments, (d and e) blocky shards with smooth conchoidal (curved) fracture surfaces, and (f) occasional anhydrite particles with sharp edges, angular joints, and smooth surfaces indicating only minimal dissolution.

plume samples for a number of reasons. First, the finer sulfur particles appear to be formed in the heat-driven, buoyantly rising magmatic-hydrothermal fluids and carried upward to the plumes over the summit, which are highly enriched in elemental sulfur (Figure 7). Second, while it is insoluble in water, elemental sulfur might be subject to chemical or microbial oxidation. Third, the absence of elemental sulfur in the deep plumes may be a result of sampling limitations. It is difficult to sample much closer than about 20 m above the seafloor when conducting CTD tow-yos over steeply shoaling or deepening terrain. There is no quantitative information about the size distribution of sulfur spherules in the loose deposits near Brimstone Pit and elsewhere near the summit, but they may be large enough to avoid suspension to the distance above the seafloor sampled during the tows, even in a vigorous sediment gravity flow. Additionally, elemental sulfur particles may be present, but in such a proportionally low quantity relative to the ash that their detection by SEM may be hindered by the rapid sublimation of elemental sulfur under the high vacuum during imaging. There is also the possibility that the absence of elemental sulfur in the deep plumes might be an indication that the plumes originated by collapse of an eruption column, as base surges due to explosions, or another presently unrecognized process that mechanically separates volcaniclasts from other products during the eruption.

[27] Results from NW Rota-1 can be compared to the style and circumstances of ash production and dispersal at the shallow submarine Myojinsho eruption of 1952–1953 [*Fiske et al.*, 1998] and as predicted by various models. The Myojinsho eruption was very near the ocean surface and its subaerial features were extensively observed. Later studies combined the detailed information about the eruption with new bathymetry and side-scan sonar imagery to infer the submarine modes of ash transport [*Fiske et al.*, 1998]. NW Rota-1 shares some common characteristics with Myojinsho: both are symmetrical, steep-sided, cone-shaped edifices with volcaniclastic aprons that display linear patterns in side-scan sonar images. *Fiske et al.* [1998] interpret the lineations along the flanks of Myojinsho as channels and levees formed by the repeated passage of sediment gravity flows. They concluded sediment gravity flows were likely initiated during the 1952–1953 eruption by several mechanisms: vertical density currents that formed when air fall ash became highly concentrated in the surface layer around the summit, explosive destruction of lava domes that repeatedly formed and disappeared during the 12.5 month eruption, and tsunami energy that may have been strong enough to remobilize fine deposits on the steep flanks of the volcano.

[28] *Head and Wilson* [2003] model several eruption styles to infer how various volcanic deposits are formed.
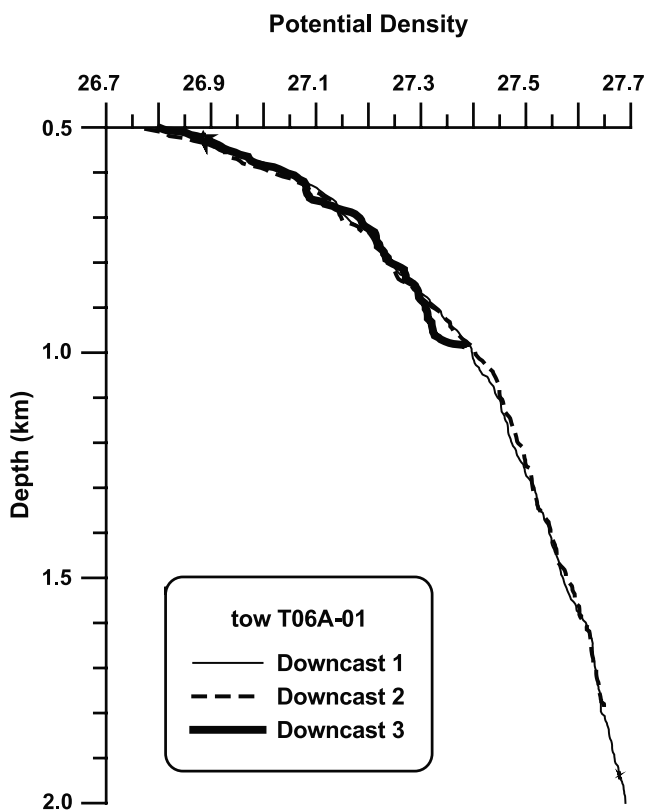
**Potential Density**



**Figure 10.** Potential density profiles from the downcast portions of T06A-01 through deep plume layers. The density profile for downcast 3 has lower density (similar to water about 50 m shallower) between 900 and 970 m than the density profiles for downcast 1 or downcast 2. This suggests that water from higher in the water column has been drawn downslope by entrainment in a sediment gravity flow.

They find that Strombolian and Hawaiian eruptions account for pyroclastic deposits in many deep sea settings. They suggest that Strombolian eruptions will be intermittent, have low effusion rates, and are unlikely to have a volume density of particles in eruption columns that will produce extensive sediment gravity flows. Hawaiian and modified Hawaiian style eruptions are more continuous eruptions of high gas content magma and will produce eruption columns dense enough to generate sediment gravity flows that spread laterally up to ~1 km (without taking into account the slope of the seafloor). *Chadwick et al.* [2008] describe the eruptive activity at NW Rota-1 as Strombolian. Evidently, the prolonged duration of the eruption and presence of deep plumes suggest sediment gravity flows are more likely with this eruption style and distribute volcaniclastic materials farther than predicted by *Head and Wilson* [2003].

## 7. Fate of Ash in Deep Plumes

[29] After detaching from the flanks of NW Rota-1, the deep particle plumes transport ash horizontally making it available for deposition in distal sediments by settling of individual particles or aggregates. These particle layers are found throughout the water column deeper than about 600 m in all directions around NW Rota-1 and are consistent with

the dispersal of sediment clouds after run-out or lift-off of sediment gravity flows (see Appendix A). Multiple plume layers may indicate multiple gravity flow events each with different source volumes, concentrations, and momentum, or may result from the progressive disintegration of a single flow. The lack of a strong directional distribution for the deep plumes suggests the sediment gravity flows spread radially as they progress down the flanks of the volcano without prominent bathymetric features to channel them in specific directions [*Dade and Huppert*, 1995; *Fiske et al.*, 1998]. Regional currents may not be strong enough to redirect the plumes in the short term, or mean flow may be altered and trapped into circumferential patterns around the volcano as at other seamounts [*Lavelle et al.*, 2003; *Codiga*, 1993; *Eriksen*, 1991].

[30] The distribution of these plumes can also be compared to patterns of intermediate nepheloid layers (INLs) common on continental slopes and in submarine canyons [e.g., *Cacchione and Drake*, 1986; *Hickey et al.*, 1986; *Kineke et al.*, 2000; *Xu et al.*, 2002]. INLs are often observed at the depth of the continental slope break or other topographic lift-off points, equivalent to mesopycnal flows in the classification system of *Mulder and Alexander* [2001]. However, other mechanisms have been considered for the formation of INLs along continental shelves, and these processes may also act to remove ash from downslope transport at NW Rota-1.

[31] Several studies have observed that INLs are often present at a depth coincident with topography on the slope that is critical (where the slope of an internal wave is identical to the slope of the boundary) for reflection of semidiurnal ($M_2$) internal tides [*Thorpe and White*, 1988; *McPhee-Shaw and Kunze*, 2002; *McPhee-Shaw*, 2006]. Internal wave reflection causes boundary layer turbulence, increasing the energy available for resuspending sediments, mixing the local vertical density gradient, and leading to horizontal advection (INL intrusion) as the fluids seek to reestablish density stratification (gravitational collapse).

[32] The slopes at NW Rota-1 over the depth range where the most prominent deep plumes extend away from the flanks are far steeper than continental slope boundaries (~30° compared to 1−3° at continental slopes) making them critical for internal waves with frequencies on the order of 1−6 h, much different than for $M_2$ internal tides (~12 h) [*McPhee-Shaw*, 2006]. While internal waves with 1−6 h frequencies may be present, energy from internal wave reflection is not required to resuspend sediments or create boundary layer instabilities here. Sediment gravity flows are vertically unstable, with vigorous turbulent mixing near the head of the flow (see Appendix A), thereby providing a readily available source of energy and suspended particles at the slope boundary. Horizontal intrusions can result from this vertical mixing and disturbance of density stratification as the flow travels downslope without relying on internal wave reflection, thereby spreading ash away from the flanks of the volcano.

[33] Many fine ash layers in sediments around oceanic arcs have been attributed to fall out of airborne tephra from subaerial eruptions [e.g., *Fujioka et al.*, 1992; *Lee et al.*, 1995; *Clift and Lee*, 1998]. Our study shows that ash from an active submarine eruption can be transported through the water column to enter distal sediments even in the absence

of a subaerial eruption. We can estimate the amount of ash available for deposition via this route from these observations. The ash distribution changed little over a 6 week period in 2004 [*Embley et al.*, 2006a]. Concentrations were lower in 2006 with a more rapid decrease over a 6-day period. A critical unknown is the rate at which this material is replenished. However, these eruptions appear to continuously contribute to a persistent ash layering completely surrounding the volcano with a mean mass load of $\sim 1-3 \times 10^6$ kg at any one time, based on the average suspended mass concentrations derived from $\Delta$NTU measurements over the depth interval between 600 m and the 2000 m bathymetric contour (a radial distance of $\sim 4$ km from the summit) during 2004 and 2006. Assuming a wet density of 1.7 g cm$^{-3}$ (a typical wet density of ash-rich sediments near the Mariana volcanic arc [*Shipboard Scientific Party*, 1981]), yields about 700–2000 m$^3$ of ash.

[34] No long-term current meter measurements are available from the waters around NW Rota-1, but a transit line of ADCP profiles was acquired in 1994 along 143°E [*Kaneko et al.*, 1998]. Currents at $\sim 700$ m (near the depth limit of the ADCP) between 10 and 15°N were dominantly E-W with nominal speeds of $\sim 5$ cm s$^{-1}$ in the E-W direction (no N-S component was given). *Fiske et al.* [1998] report speeds of 20 cm s$^{-1}$ at 773 m near Myojin Knoll volcano in the Izu-Bonin arc at 32°N. Assuming nominal current speeds of 1 to 5 cm s$^{-1}$, an average suspended ash concentration of 0.08 mg L$^{-1}$, and a cross section area of $2.8 \times 10^6$ m$^2$ (4 km wide by 1400 m thick, passing through the volcano axis), a yearly flux of 0.7 to $3.5 \times 10^8$ kg of ash could be made available for widespread distribution to fall-out deposits, equivalent to 0.4 to $2.0 \times 10^5$ m$^3$ a$^{-1}$ of wet ash volume. This equals a flux rate of 5 to 22 m$^3$ h$^{-1}$, which is comparable to the estimated lava effusion rate during eruptive phases of 1–100 m$^3$ h$^{-1}$ for 2006 [*Chadwick et al.*, 2008]. Eruptive bursts observed at Brimstone Pit in 2006 were cyclic and emplacement of fine ash into the water column is also probably episodic (coinciding with active eruptive phases). However, during the 2003–2006 period, NW Rota-1 appears to have been experiencing long-term, possibly near-continuous eruptions. Ash input of the magnitude seen here over the scale of months to years during periods of eruptive activity could account for millimeter-thick ash layers as recorded in many sediment cores [e.g., *Fujioka et al.*, 1992; *Lee et al.*, 1995; *Clift and Lee*, 1998]. Previous interpretations that ash layers in sediment cores collected in the vicinity of oceanic arcs are the result only of subaerial eruptions, or that they delineate specific events, may need to be reexamined. These results offer the possibility that fall-out ash deposits might more commonly originate from the submarine component of regional volcanism.

## 8. Summary

[35] Repeat bathymetric surveys and the distribution and composition of particle plumes around NW Rota-1 provide valuable evidence of how explosive eruptions contribute to the construction of a submarine volcano and supply ash to the surrounding environment. Magmatic-hydrothermal emissions are separated buoyantly from explosively generated volcaniclastic products. This was seen by direct observation at the vent [*Deardorff et al.*, 2006] and in the dissolved and particulate composition of the plumes. Sediment gravity flows transport volcaniclastic materials down the flanks of the volcano. Between 2003 and 2006 a volume of $3.3 \times 10^7$ m$^3$ of new material was added to the southern flank, downslope of the eruptive vent, in a deposit that extended 4 km from the summit. Fine ash was carried farther and was still suspended in near-bottom nepheloid layers at distances up to tens of kilometers away.

[36] Ash was also dispersed to the midwater column in all directions surrounding the volcano and illustrates a different mode of transport than previously considered. Particle-rich intrusions detach from the slopes of the volcano as sediment gravity flows loose momentum (run-out), loose bulk density (lift-off), or create horizontal intrusions as vertical mixing causes gravitational collapse in a stratified environment. These layers can be coherent for several kilometers, with mass flux of ash through the water similar to the amount of lava extruded by the eruption and deposited proximally. This process can remove a significant portion of the erupted material making it available for deposit in more distal sediments.

## Appendix A: Sediment Gravity Flow Terminology

[37] The terminology for gravity flows, also called density flows or currents, is neither well established nor consistently used in the geological literature. Gravity flows generally refer to a wide range of mass transport events, occurring subaerially or subaqueously, where mixtures of solid particles and fluid are subject to movement caused by gravity acting on the grains within the mixture, and by differences in bulk density between the mixture and ambient fluid. Classification schemes generally define sediment gravity flows as those where particle movement drives movement of the interstitial fluid, and fluid gravity flows as those where suspended solid transport is incidental to the gravity-driven movement of the fluid [e.g., *Middleton and Hampton*, 1976; *Mulder and Alexander*, 2001; *Simpson*, 1987].

[38] For the subaqueous environment, *Middleton and Hampton* [1976] proposed a classification system based on the mechanisms of suspension and interaction of the solids within the mixture. They used the terms debris flow, grain flow, fluidized sediment flow, and turbidity current to encompass a wide range of conditions for grain size and modes of support maintaining the grains in suspension. They further distinguished sediment gravity flows from slumps and slides, which have greater cohesion of the sediments and little or no internal deformation of the transported mass upon deposition. *Mulder and Alexander* [2001] base their classification system on cohesivity of the grains, flow duration, and sediment concentration in addition to mechanisms for particle suspension. They also differentiate flows by their bulk density relative to the density of the ambient fluid (i.e., homopycnal, mesopycnal, hypopycnal, and hyperpycnal conditions). However, any given sediment gravity flow event may have properties that span entire classification systems across spatial dimensions and with time [*Fisher*, 1983; *Mulder and Alexander*, 2001; *Amy et al.*, 2005] and may transform from one type of

gravity flow to another [e.g., *Hampton*, 1972]; so as a practical matter, distinctions can become blurred [*Middleton and Hampton*, 1976].

[39] The term turbidity current, also called turbidity flows, usually refers to more dilute flows with sediment concentrations supported in suspension by turbulence of the fluid, and has been defined theoretically as flows with volume concentrations <9% solids [*Bagnold*, 1962]. However, this term is often used where volume concentrations are much greater or without quantifying sediment concentrations. For example, turbidity currents are considered responsible for emplacement of turbidite sediment fans at the base of continental slopes and submarine canyons and for mass transport events that can travel at high speeds and have been known to cause destruction to submarine cables and moorings [e.g., *Lowe*, 1982; *Paull et al.*, 2003; *Garfield et al.*, 1994; *Khripounoff et al.*, 2003].

[40] Sediment gravity flows are generally composed of head, body and tail regions that have well known characteristics of turbulence and mixing over some thickness above a boundary [*Simpson*, 1987; *Middleton and Hampton*, 1976], and result in radial distribution patterns when not constrained by channels or other boundary geometry [*Dade and Huppert*, 1995; *Simpson*, 1987]. Some fraction of fine-grained particles are lost to the overlying fluid in eddies and by diffusion (elutriation), to be dispersed more widely by regional currents before entering distal deposits via settling of individual particles (i.e., fall-out deposits). Solids can also be lost by deposition directly from the flow. Erosion of sediments under the head and body can cause previously deposited material to be remobilized and transported with the flow. Run-out distances depend on several factors, but only slight slopes are necessary to allow dilute concentrations of suspended sediments to propagate for tens of kilometers in the submarine environment [*Middleton and Hampton*, 1976; *Dade and Huppert*, 1995]. The combined effects of dissolution and deposition act to diminish the bulk density of sediment gravity flows. At some point, the flow will stop (run-out), or as the flow progresses, portions of the more dilute cloud surrounding the flow may become neutrally buoyant, or positively buoyant if the density difference between interstitial and ambient fluid is great enough, and detach, or "liftoff," from the seafloor to spread horizontally on isopycnal surfaces that match the density of the separated cloud (i.e., the mesopycnal flows of *Mulder and Alexander* [2001] and demonstrated experimentally by *Sparks et al.* [1993]).

[41] Subaerial pyroclastic flows are examples of sediment gravity flows in which the interstitial fluid consists of hot volcanic gasses and the ambient fluid is air. Using the term pyroclastic flow in reference to subaqueous environments is controversial. It has been proposed that the term should be limited to flows of pyroclastic material that can be demonstrated to have been emplaced under hot, gas-supported conditions [*Cas and Wright*, 1991]. Other authors prefer to use the term to emphasize the origin of a deposit as the direct product of volcanic eruption regardless of thermal conditions [*Fiske et al.*, 1998; *Busby*, 2005].

[42] In this paper, we use the term sediment gravity flows, as it is the most general term that encompasses the broad range of mass transport events, including turbidity currents, and follow the criteria of *Cas and Wright* [1991] that the term pyroclastic flow should be reserved for describing hot, gas-supported flows.

## References

American Public Health Association (1985), *Standard Methods for the Examination of Water and Wastewater*, 16th ed., 1268 pp., Washington, D.C.

Amy, L. A., A. J. Hogg, J. Peakall, and P. J. Talling (2005), Abrupt transitions in gravity currents, *J. Geophys. Res.*, *110*, F03001, doi:10.1029/2004JF000197.

Bagnold, R. A. (1962), Auto-suspension of transported sediment; turbidity currents, *Proc. R. Soc. London, Ser. A*, *265*(1322), 315–319, doi:10.1098/rspa.1962.0012.

Baker, E. T., J. W. Lavelle, R. A. Feely, G. J. Massoth, S. L. Walker, and J. E. Lupton (1989), Episodic venting of hydrothermal fluids from the Juan de Fuca Ridge, *J. Geophys. Res.*, *94*, 9237–9250, doi:10.1029/JB094iB07p09237.

Baker, E. T., C. R. German, and H. Elderfield (1995), Hydrothermal plumes over spreading-center axes: Global distributions and geological inferences, in *Seafloor Hydrothermal Systems: Physical, Chemical, Biological, and Geological Interactions*, Geophys. Monogr. Ser, vol. 91, edited by S. Humphris et al., pp. 47–71, AGU, Washington, D. C.

Baker, E. T., D. A. Tennant, R. A. Feely, G. T. Lebon, and S. L. Walker (2001), Field and laboratory studies on the effect of particle size and composition on optical backscattering measurements in hydrothermal plumes, *Deep Sea Res., Part I*, *48*, 593–604, doi:10.1016/S0967-0637(00)00011-X.

Baker, E. T., G. J. Massoth, C. E. J. de Ronde, J. E. Lupton, and B. I. A. McInnes (2002), Observations and sampling of an ongoing subsurface eruption of Kavachi volcano, Solomon Islands, May 2000, *Geology*, *30*(11), 975–978, doi:10.1130/0091-7613(2002)030<0975:OASOAO>2.0.CO;2.

Baker, E. T., R. Embley, S. L. Walker, J. A. Resing, J. E. Lupton, K.-I. Nakamura, C. E. J. de Ronde, and G. Massoth (2008), Hydrothermal activity and volcano distribution along the Mariana arc, *J. Geophys. Res.*, *113*, B08S09, doi:10.1029/2007JB005423.

Bowers, T. S., K. L. Von Damm, and J. M. Edmond (1985), Chemical evolution of mid-ocean ridge hot springs, *Geochim. Cosmochim. Acta*, *49*, 2239–2252, doi:10.1016/0016-7037(85)90224-8.

Busby, C. (2005), Possible distinguishing characteristics of very deepwater explosive and effusive silicic volcanism, *Geology*, *33*(11), 845–848, doi:10.1130/G21216.1.

Butterfield, D. A., I. R. Jonasson, G. J. Massoth, R. A. Feely, K. K. Roe, R. E. Embley, J. F. Holden, R. E. McDuff, M. D. Lilley, and J. R. Delaney (1997), Seafloor eruptions and evolution of hydrothermal fluid chemistry, *Philos. Trans. R. Soc. London, Ser. A*, *355*, 369–386, doi:10.1098/rsta.1997.0013.

Cacchione, D. A., and D. E. Drake (1986), Nepheloid layers and internal waves over continental shelves and slopes, *Geo Mar. Lett.*, *6*, 147–152, doi:10.1007/BF02238085.

Carey, S. (1997), Influence of convective sedimentation on the formation of widespread tephra fall layers in the deep sea, *Geology*, *25*(9), 839–842, doi:10.1130/0091-7613(1997)025<0839:IOCSOT>2.3.CO;2.

Cas, R. A. F., and J. V. Wright (1991), Subaqueous pyroclastic flows and ignimbrites: An assessment, *Bull. Volcanol.*, *53*(5), 357–380, doi:10.1007/BF00280227.

Chadwick, W. W., Jr., R. W. Embley, P. D. Johnson, S. G. Merle, S. Ristau, and A. Bobbitt (2005), The submarine flanks of Anatahan Volcano, commonwealth of the northern Mariana Islands, *J. Volcanol. Geotherm. Res.*, *146*, 8–25, doi:10.1016/j.jvolgeores.2004.11.032.

Chadwick, W. W., Jr., K. V. Cashman, R. W. Embley, H. Matsumoto, R. P. Dziak, C. E. J. de Ronde, T. K. Lau, N. Deardorff, and S. G. Merle (2008), Direct video and hydrophone observations of submarine explosive eruptions at NW Rota-1 volcano, Mariana Arc, *J. Geophys. Res.*, *113*, B08S10, doi:10.1029/2007JB005215.

Chiminée, J.-L., P. Stoffers, G. McMurty, H. Richnow, D. Puteanus, and P. Sedwick (1991), Gas-rich submarine exhalations during the 1989 eruption of Macdonald Seamount, *Earth Planet. Sci. Lett.*, *107*, 318–327, doi:10.1016/0012-821X(91)90079-W.

Clague, D. A., A. S. Davis, J. L. Bischoff, J. E. Dixon, and R. Geyer (2000), Lava bubble-wall fragments formed by submarine hydrovolcanic

explosions on Loihi Seamount and Kilauea Volcano, *Bull. Volcanol.*, *61*, 437–449, doi:10.1007/PL00008910.

Clague, D. A., R. Batiza, J. W. Head III, and A. S. Davis (2003), Pyroclastic and hydroclastic deposits on Loihi Seamount, Hawaii, in *Explosive Subaqueous Volcanism*, *Geophys. Monogr. Ser.*, vol. 140, edited by J. D. L. White, J. L. Smellie, and D. A. Clague, pp. 73–95, AGU, Washington, D.C.

Clift, P. D., and J. Lee (1998), Temporal evolution of the Mariana Arc during rifting of the Mariana Trough traced through the volcaniclastic record, *Isl. Arc*, *7*, 496–512, doi:10.1111/j.1440-1738.1998.00206.x.

Codiga, D. L. (1993), Laboratory realizations of stratified seamount-trapped waves, *J. Phys. Oceanogr.*, *23*, 2053–2071, doi:10.1175/1520-0485(1993)023<2053:LROSST>2.0.CO;2.

Dade, W. B., and H. E. Huppert (1995), Runout and fine-sediment deposits of axisymmetric turbidity currents, *J. Geophys. Res.*, *100*(C9), 18,597–18,609, doi:10.1029/95JC01917.

Deardorff, N., W. W. Chadwick Jr., R. W. Embley, and K. V. Cashman (2006), Submarine explosive eruptions: Physical volcanology of NW Rota-1, Marianas, *Eos Trans. AGU*, *87*(52), Fall Meet. Suppl., Abstract V23B–0609.

de Ronde, C. E. J., G. J. Massoth, E. T. Baker, and J. E. Lupton (2003), Submarine hydrothermal venting related to volcanic arcs, in *Volcanic, Geothermal, and Ore-forming Fluids: Rulers and Witnesses of Processes Within the Earth*, edited by S. F. Simmons and I. Graham, *Spec. Publ. Soc. Econ. Geol.*, *10*, 91–110.

de Ronde, C. E. J., et al. (2005), Evolution of a submarine magmatic-hydrothermal system: Brothers Volcano, southern Kermadec arc, New Zealand, *Econ. Geol.*, *100*, 1097–1133, doi:10.2113/100.6.1097.

de Ronde, C. E. J., et al. (2007), Submarine hydrothermal activity along the mid-Kermadec arc, New Zealand: Large-scale effects on venting, *Geochem. Geophys. Geosyst.*, *8*, Q07007, doi:10.1029/2006GC001495.

Draut, A. E., and P. D. Clift (2006), Sedimentary processes in modern and ancient oceanic arc settings: Evidence from the Jurassic Telketna formation of Alaska and the Mariana and Tonga arcs, western Pacific, *J. Sediment. Res.*, *76*, 493–514, doi:10.2110/jsr.2006.044.

Embley, R. W., E. T. Baker, W. W. Chadwick Jr., J. E. Lupton, J. E. Resing, G. J. Massoth, and K. Nakamura (2004), Explorations of Mariana Arc volcanoes reveal new hydrothermal systems, *Eos Trans. AGU*, *85*(4), 37–44, doi:10.1029/2004EO040001.

Embley, R. W., et al. (2006a), Long-term eruptive activity at a submarine arc volcano, *Nature*, *441*(7092), 494–497, doi:10.1038/nature04762.

Embley, R. W., W. W. Chadwick Jr., R. J. Stern, S. G. Merle, S. H. Bloomer, K. Nakamura, and Y. Tamura (2006b), A synthesis of multibeam bathymetry and backscatter, and sidescan sonar of the Mariana submarine magmatic arc, western Pacific, *Eos Trans. AGU*, *87*(52), Fall Meet. Suppl., Abstract V41B–1723.

Eriksen, C. C. (1991), Observations of amplified flows atop a large seamount, *J. Geophys. Res.*, *96*(C8), 15,227–15,236, doi:10.1029/91JC01176.

Feely, R. A., M. Lewison, G. J. Massoth, G. Robert-Baldo, J. W. Lavelle, R. H. Byrne, K. L. Von Damm, and H. C. Curl Jr. (1987), Composition and dissolution of black smoker particulates from active vents on the Juan de Fuca Ridge, *J. Geophys. Res.*, *92*(B11), 11,347–11,363, doi:10.1029/JB092iB11p11347.

Feely, R. A., E. T. Baker, G. T. Lebon, J. F. Gendron, J. A. Resing, and J. P. Cowen (1999), Evidence for iron and sulfur enrichments in hydrothermal plumes at Axial Volcano following the January–February 1998 eruption, *Geophys. Res. Lett.*, *26*(24), 3649–3652, doi:10.1029/1999GL002325.

Fisher, R. V. (1983), Flow transformations in sediment gravity flows, *Geology*, *11*, 273–274, doi:10.1130/0091-7613(1983)11<273:FTISGF>2.0.CO;2.

Fiske, R. S., K. V. Cashman, A. Shibata, and K. Watanabe (1998), Tephra dispersal from Myojinsho, Japan, during its shallow submarine eruption of 1952–1953, *Bull. Volcanol.*, *59*, 262–275, doi:10.1007/s004450050190.

Fox, C. G., W. W. Chadwick Jr., and R. W. Embley (1992), Detection of changes in ridge-crest morphology using repeated multibeam sonar surveys, *J. Geophys. Res.*, *97*, 11,149–11,162, doi:10.1029/92JB00601.

Fryer, P., J. B. Gill, and M. C. Jackson (1997), Volcanologic and tectonic evolution of the Kasuga seamounts, northern Mariana Trough: Alvin submersible investigations, *J. Volcanol. Geotherm. Res.*, *79*, 277–311, doi:10.1016/S0377-0273(97)00013-9.

Fujioka, K., Y. Matsuo, A. Nishimura, M. Koyama, and K. S. Rodolfo (1992), Tephras of the Izu-Bonin forearc (sites 787, 792, and 793), *Proc. Ocean Drill. Program Sci. Results*, *126*, 47–74.

Garfield, N., T. A. Rago, K. J. Schnebele, and C. A. Collins (1994), Evidence of a turbidity current in Monterey Submarine Canyon associated with the 1989 Loma Prieta earthquake, *Cont. Shelf Res.*, *14*(6), 673–686, doi:10.1016/0278-4343(94)90112-0.

Hampton, M. A. (1972), The role of subaqueous debris flow in generating turbidity currents, *J. Sediment. Petrol.*, *42*(4), 775–793.

Head, J. W., III, and L. Wilson (2003), Deep submarine pyroclastic eruptions: Theory and predicted landforms and deposits, *J. Volcanol. Geotherm. Res.*, *121*, 155–193, doi:10.1016/S0377-0273(02)00425-0.

Hickey, B., E. T. Baker, and N. Kachel (1986), Suspended particle movement in and around Quinault submarine canyon, *Mar. Geol.*, *71*, 35–83, doi:10.1016/0025-3227(86)90032-0.

Kaneko, I., Y. Takasuki, H. Kamiya, and S. Kawae (1998), Water property and current distributions along the WHP-P9 section (137°–142°E) in the western North Pacific, *J. Geophys. Res.*, *103*(C6), 12,959–12,984, doi:10.1029/97JC03761.

Khripounoff, A., A. Vangriesheim, N. Babonneau, P. Crassous, B. Dennielou, and B. Savoye (2003), Direct observation of intense turbidity current activity in the Zaire submarine valley at 4000 m water depth, *Mar. Geol.*, *194*, 151–158, doi:10.1016/S0025-3227(02)00677-1.

Kineke, G. C., K. J. Woolfe, S. A. Kuehl, J. D. Milliman, T. M. Dellapenna, and R. G. Purdon (2000), Sediment export from the Sepik River, Papua New Guinea: Evidence for a divergent sediment plume, *Cont. Shelf Res.*, *20*(16), 2239–2266, doi:10.1016/S0278-4343(00)00069-8.

Kokelaar, P., and C. Busby (1992), Subaqueous explosive eruption and welding of pyroclastic deposits, *Science*, *257*(5067), 196–201, doi:10.1126/science.257.5067.196.

Kuhn, T., P. M. Herzig, M. D. Hannington, D. Garbe-Schonberg, and P. Stoffers (2003), Origin of fluids and anhydrite precipitation in the sediment-hosted Grimsey hydrothermal field north of Iceland, *Chem. Geol.*, *202*, 5–21, doi:10.1016/S0009-2541(03)00207-9.

Lavelle, J. W., E. T. Baker, and G. A. Cannon (2003), Ocean currents at Axial Volcano, a northeastern Pacific seamount, *J. Geophys. Res.*, *108*(C2), 3020, doi:10.1029/2002JC001305.

Lebon, G., J. Resing, E. Baker, R. Embley, and J. Lupton (2004), Chemical characteristics of plumes above and around NW Rota Submarine volcano: Before and during the March 2004 eruption, *Eos Trans. AGU*, *85*(47), Fall Meet. Suppl., Abstract V41B-1386.

Lee, J., R. J. Stern, and S. H. Bloomer (1995), Forty million years of magmatic evolution in the Mariana Arc: The tephra glass record, *J. Geophys. Res.*, *100*, 17,671–17,687, doi:10.1029/95JB01685.

Limén, H., S. K. Juniper, V. Tunnicliffe, and M. Clément (2006), Benthic community structure on two peaks of an erupting seamount: Northwest Rota-1 volcano, Mariana Arc, western Pacific, *Cah. Biol. Mar.*, *47*, 457–463.

Lowe, D. R. (1982), Sediment gravity flows: II. Depositional models with special reference to the deposits of high-density turbidity currents, *J. Sediment. Petrol.*, *52*(1), 279–297.

Lupton, J. L., and H. Craig (1975), Excess $^3$He in oceanic basalts: Evidence for terrestrial primordial helium, *Earth Planet. Sci. Lett.*, *26*, 133–139, doi:10.1016/0012-821X(75)90080-1.

Mandeville, C. W., S. Carey, and H. Sigurdsson (1996), Sedimentology of the Krakatau 1883 submarine pyroclatic deposits, *Bull. Volcanol.*, *57*(7), 512–529.

Manville, V., and C. N. J. Wilson (2004), Vertical density currents: A review of their potential role in the deposition and interpretation of deep-sea ash layers, *J. Geol. Soc.*, *161*, 947–958, doi:10.1144/0016-764903-067.

McPhee-Shaw, E. (2006), Boundary-interior exchange: Reviewing the idea that internal-wave mixing enhances lateral dispersal near continental margins, *Deep Sea Res., Part II*, *53*, 42–59, doi:10.1016/j.dsr2.2005.10.018.

McPhee-Shaw, E. E., and E. Kunze (2002), Boundary layer intrusions from a sloping bottom: A mechanism for generating intermediate nepheloid layers, *J. Geophys. Res.*, *107*(C6), 3050, doi:10.1029/2001JC000801.

Middleton, G. V., and M. A. Hampton (1976), Subaqueous sediment transport and deposition by sediment gravity flows, in *Marine Sediment Transport and Environmental Management*, edited by D. J. Stanley and D. J. P. Swift, pp. 197–218, J. Wiley, New York.

Mulder, T., and J. Alexander (2001), The physical character of subaqueous sedimentary density flows and their deposits, *Sedimentology*, *48*, 269–299, doi:10.1046/j.1365-3091.2001.00360.x.

Paull, C. K., W. Ussler III, H. G. Greene, R. Keaten, P. Mitts, and J. Barry (2003), Caught in the act: The 20 December 2001 gravity flow event in Monterey Canyon, *Geo Mar. Lett.*, *22*, 227–232, doi:10.1007/s00367-003-0117-2.

Resing, J. A., R. A. Feely, G. J. Massoth, and E. T. Baker (1999), The water-column chemical signature after the 1998 eruption of Axial Volcano, *Geophys. Res. Lett.*, *26*(24), 3645–3648, doi:10.1029/1999GL002350.

Resing, J. A., G. Lebon, E. T. Baker, J. E. Lupton, R. W. Embley, G. J. Massoth, W. W. Chadwick Jr., and C. E. J. de Ronde (2007), Venting of acid-sulfate fluids in a high-sulfidation setting at NW Rota-1 submarine volcano on the Mariana Arc, *Econ. Geol.*, *102*(6), 1047–1061, doi:10.2113/gsecongeo.102.6.1047.

Shipboard Scientific Party (1981), Site 455: East side of the Mariana Trough, *Initial Rep. Deep Sea Drill. Proj.*, *60*, 203–213.

Sigurdsson, H., et al. (2006), Marine investigations of Greece's Santorini volcanic field, *Eos Trans. AGU*, *87*(34), 337, doi:10.1029/2006EO340001.

Simpson, J. E. (1987), *Gravity Currents in the Environment and the Laboratory*, 244 pp., Ellis Horwood, Chichester, U. K.

Sparks, R. S. J., R. T. Bonnecaze, H. E. Huppert, J. R. Lister, M. A. Hallworth, H. Mader, and J. Phillips (1993), Sediment-laden gravity currents with reversing buoyancy, *Earth Planet. Sci. Lett.*, *114*(2–3), 243–257, doi:10.1016/0012-821X(93)90028-8.

Stern, R. J., M. J. Fouch, and S. Klemperer (2003), An overview of the Izu-Bonin-Mariana subduction factory, in *Inside the Subduction Factory*, *Geophys. Monogr. Ser*, vol. 138, edited by J. Eiler and M. Hirschmann, pp. 175–222, AGU, Washington, D. C.

Thorpe, S. A., and M. White (1988), A deep intermediate nepheloid layer, *Deep Sea Res.*, *35*(9), 1665–1671, doi:10.1016/0198-0149(88)90109-4.

White, D. L. (2000), Subaqueous eruption-fed density currents and their deposits, *Precambrian Res.*, *101*, 87–109, doi:10.1016/S0301-9268(99)00096-0.

White, J. D. L., J. L. Smellie, and D. A. Clague (2003), Introduction: A deductive outline and topical overview of subaqueous explosive volcanism, in *Explosive Subaqueous Volcanism*, *Geophys. Monogr. Ser.*, vol. 140, edited by J. D. L. White, J. L. Smellie, and D. A. Clague, pp. 1–23, AGU, Washington, D. C.

Wright, I. C. (1996), Volcaniclastic processes on modern submarine arc stratovolcanoes: Sidescan and photographic evidence from the Rumble IV and V volcanoes, southern Kermadec arc (SW Pacific), *Mar. Geol.*, *136*, 21–39, doi:10.1016/S0025-3227(96)00054-0.

Wright, I. C., W. Chadwick, C. E. J. de Ronde, D. Reymond, O. Hyvernaud, H.-H. Gennerich, P. Stoffers, K. Mackay, M. Dunkin, and S. Bannister (2008), Collapse and reconstruction of Monowai submarine volcano, Kermadec arc, 1998–2004, *J. Geophys. Res.*, *113*, B08S03, doi:10.1029/2007JB005138.

Xu, J. P., M. Noble, S. L. Eittreim, L. K. Rosenfeld, F. B. Schwing, and C. H. Pilskaln (2002), Distribution and transport of suspended particulate matter in Monterey Canyon, California, *Mar. Geol.*, *181*(1–3), 215–234, doi:10.1016/S0025-3227(01)00268-7.

_____

E. T. Baker and S. L. Walker, PMEL NOAA, 7600 Sand Point Way NE, Seattle WA 98115, USA. (sharon.l.walker@noaa.gov)

W. W. Chadwick Jr. and S. G. Merle, CIMRS, Oregon State University, 2115 SE OSU Drive, Newport, OR 97365, USA.

G. T. Lebon and J. A. Resing, JISAO, University of Washington, 7600 Sand Point Way NE, Seattle, WA 98195, USA.

J. E. Lupton, PMEL NOAA, 2115 SE OSU Drive, Newport, OR 97365, USA.